Submitted to
32nd International Conference on High Energy Physics, ICHEP04, August 16, 2004, Beijing
Abstract: **5-0172**
Parallel Session **5**
www-h1.desy.de/h1/www/publications/conf/conf_list.html

Forward Jet Production at HERA

H1 Collaboration

Abstract

The cross section for inclusive forward jet production in ep collisions at HERA is presented as a function of x_{Bj}, as is a measurement of the triple differential cross section $\frac{d^3\sigma}{dx\,dQ^2\,dp^2_{t,jet}}$ which covers the phase space from the "direct photon" region ($Q^2 \gg p^2_{t,jet}$) to the "resolved virtual photon" region ($Q^2 \ll p^2_{t,jet}$) via the "BFKL region" ($Q^2 \sim p^2_{t,jet}$). In addition, cross sections for events with a central di-jet system in addition to the forward jet are shown as a function of the rapidity separation between the forward jet and the two central jets. The measurements are compared with the predictions of next-to-leading order QCD calculations and various QCD-based models; some of these generate parton emissions ordered in virtuality while others produce non-ordered emissions.

1 Introduction

The hadronic final state in deep inelastic scattering offers an extensive field of research for QCD phenomena. This includes studies of hard parton emissions which result in well defined jets, semi-hard perturbative effects responsible for multiple gluon emissions and the non-perturbative hadronization process.

HERA has extended the available x_{Bj} region down to values of $x_{Bj} \simeq 10^{-4}$, for values of the momentum transfer, Q^2, larger than a few GeV^2, where perturbative calculations in QCD are still expected to be valid. At these low x_{Bj} values, a parton in the proton can induce a QCD cascade, consisting of several subsequent parton emissions, before eventually an interaction with the virtual photon takes place. QCD calculations based on "direct" interactions between a point-like photon and a parton from an evolution chain as given by the DGLAP scheme [1], have been successful in reproducing the strong rise of $F_2(x_{Bj}, Q^2)$ with decreasing x_{Bj}. On the other hand, significant deviations from the simple LO DGLAP approach have been observed in data on the fractional rate of di-jet events, inclusive jet production, transverse energy flow and $p_{t,jet}$ spectra of charged particles. Going from LO to NLO allowed some of the deviations to be resolved, but in specific regions of phase space the description of the measurements are still unsatisfactory.

The colour dipole model (CDM) [2], which assumes that the gluon emission originates from independently radiating colour dipoles, is in fairly good agreement with these data. This suggests that new parton dynamics, not included in the LO DGLAP approach, are responsible for the observed deviations. However, further investigations made clear that ascribing partonic structure to the virtual photon and considering so called resolved photon processes is similar to a full NLO calculation [3]. Including leading log parton showers from both the photon and the proton side leads to a rather satisfactory description of the data. Thus, more sophisticated measurements are necessary to establish the existence of new parton dynamics.

In this analysis we have studied events where a jet has been produced in the forward direction (the angular region close to the incoming proton), a region which typically lies well away from the photon end of the evolution ladder. By applying various cuts we have tried to suppress DGLAP evolution in order to become more sensitive to new parton dynamics. Comparisons of data have been made with next-to-leading order (NLO) calculations and several QCD models. In this analysis the DISENT program [4] has been used to investigate the level of agreement between the forward jet data and NLO calculations.

2 QCD-models

At high energies the phase space available for emissions is large. Higher order QCD effects will therefore become important and in order to account for these it is necessary to use phenomenological models. There are various models on the market with different approximations to the full evolution equations for parton branchings, which lead to observable differences in the predictions for the details of parton cascade.

The most frequently used description so far is given by the DGLAP evolution equations, which corresponds to the assumption that the leading contribution comes from strong ordering in the virtualities of the parton propagators in the evolution chain, with the largest virtualities reached in the hard scattering with the point-like photon. Compared to the hard scale the propagator virtualities can be neglected, so that the propagators can be assumed to be collinear with the incoming proton (collinear approach). The interaction is assumed to take place with a point-like photon (DGLAP direct).

In events where the scale of the hard subprocess is larger than Q^2, the structure of the virtual photon might be resolved and the interaction takes place with one of the partons in the photon. This is described within the DGLAP model by introducing two evolution ladders, one from the photon side and one from the proton side, and is called the resolved photon model [5] (DGLAP resolved).

The DGLAP approximation neglects contributions from terms dependent on powers of $\log(1/x)$, which appear in the full evolution equation, where x is the longitudinal momentum fraction of the propagating parton. At small enough x-values, these terms eventually dominate over the $\log(Q^2)$ terms which are considered by DGLAP. In the small x_{Bj} region, the DGLAP description is thus expected to break down and the parton dynamics should instead be given by the BFKL evolution equations [6], which resum $\log(1/x)$ terms to all orders in the coupling constant. This model gives strong ordering in the longitudinal momentum fraction of the propagators but no ordering in their virtualities. This means that the virtualities and the transverse momenta of the propagators can take any kinematically allowed value at each splitting. One consequence of this is that the matrix element must be taken off mass-shell and convoluted with parton distributions which take the transverse momenta of the propagators into account (unintegrated parton densities).

The CCFM equation [7] provides a bridge between the DGLAP and BFKL descriptions by resumming terms in both $\log(Q^2)$ and $\log(1/x)$, which should make it valid in the complete x range. In the CCFM model the real emissions are ordered in angle, which gives a correct treatment of colour coherence effects. The factorization scale is determined by the rescaled transverse momentum, q, of the emitted gluons, which is related to the maximum angle, Ξ, for any emissions at the quark box connecting to the photon vertex.

A different approach to the parton evolution is given by the colour dipole model in which the emissions are generated by colour dipoles which are spanned between the partons in the cascade. Since the dipoles radiate independently there is no ordering in the transverse momenta of the emissions and the behavior is thus similar to that of the BFKL case.

3 Experimental Strategy

Differences between the various dynamic approaches to the modelling of the parton cascade are most prominent in the region close to the proton remnant direction, i.e. away from the scattered quark. This can be understood from the fact that the strong ordering in virtuality of the DGLAP description gives the softest emissions closest to the proton whereas in the BFKL model the emissions can be arbitrarily hard in this region, as long as they are kinematically allowed.

The difficulty in extracting a significant signal for BFKL dynamics is largely due to the fact that DGLAP parton evolution dominates in most of the HERA kinematic range. One way to get around this problem is to select events with a jet close to the proton direction (a forward jet) with constraints such that its transverse momentum is approximately equal to the virtuality of the photon propagator. This will suppress contributions with strong ordering in virtuality as is the case in DGLAP evolution. Experimentally, this is realized by requiring $p^2_{t,jet} \sim Q^2$, where $p^2_{t,jet}$ is the transverse momentum squared of the forward jet. If, at the same time, the forward jet is required to take a large fraction of the proton momentum, $x_{jet} = E_{jet}/E_p$, such that $x_{jet} \gg x_{Bj}$, the phase space for an evolution with ordering in the longitudinal momentum fraction, as described by BFKL, is opened up. The x_{Bj} distribution is dominated by the lower limit of the kinematic acceptance, which is close to $\sim 10^{-4}$.

Based on calculations in the Leading-Log-Approximation of the BFKL kernel, the cross section for DIS events at low x_{Bj} and large Q^2 with a forward jet [8] is expected to rise more rapidly with decreasing x_{Bj} than expected from DGLAP based calculations.

The analysis presented here is based on a statistical sample which is five times larger than that used in a previous H1 publication [9] and is complementary to a similar analysis [10] which used energetic forward pions instead of forward jets. A schematic diagram for forward jet production is shown in Fig. 1.

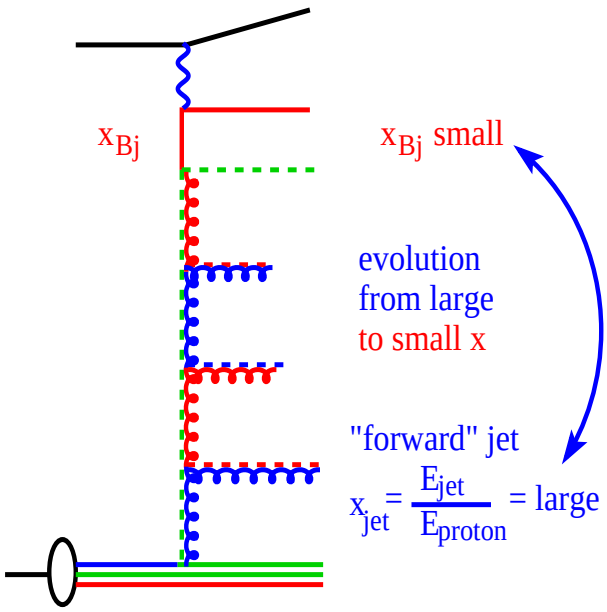

Figure 1: *Schematic diagram of an ep scattering event with a forward jet taking a fraction $x_{jet} = E_{jet}/E_p$ of the proton momentum. The evolution from large x_{jet} to small x_{Bj} is indicated. The phase space for DGLAP evolution in Q^2 is restricted by requiring $p^2_{t,jet} \sim Q^2$.*

The requirement of two high transverse momentum central jets in addition to the forward jet provides further constraints on the kinematics, in the sense that the virtuality at the end-points of the gluon ladder is known. The disadvantage is that this additional requirement gives

a significant reduction of the data sample. Schematic diagrams of such events are shown in Fig. 2 The position in rapidity space of the two central jets is relevant to the evolution. A small rapidity separation between the central jets will leave a large rapidity range for further parton radiation between the forward jet and the di-jet system, which is favourable for BFKL evolution. In contrast to this, a large rapidity separation between the central jets means that there is little room for additional emissions between the central jets and the forward jet. In this case the conditions correspond to what is expected for resolved photon processes in LO or a 3 parton final state.

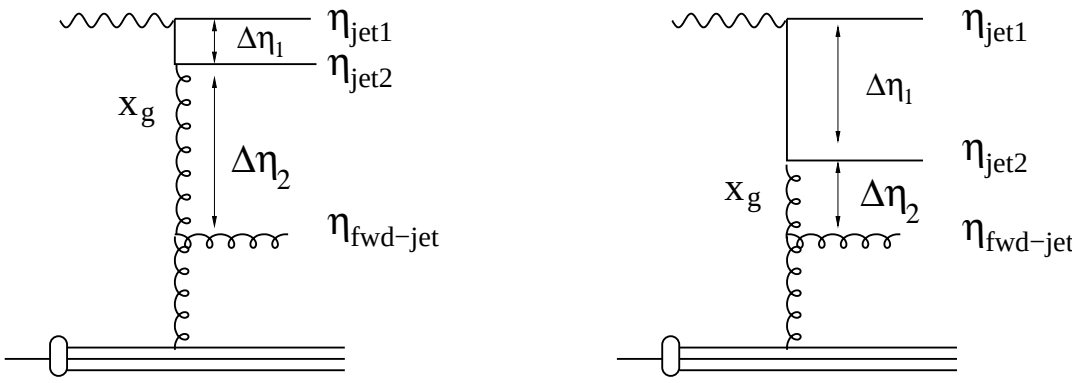

Figure 2: *Schematic diagram of an event with a forward jet and a hard di-jet system. η_i denotes the rapidity of the $i^{\rm th}$ jet, $\Delta\eta_1$ the rapidity difference between the two central jets and $\Delta\eta_2$ the rapidity difference between the hard subsystem and the forward jet. x_g is the longitudinal momentum fraction carried by the propagating gluon.*

4 The H1 Detector

A detailed description of the H1 detector can be found in [11]. The detector elements important for this analysis are described below. The kinematic variables x_{Bj} and Q^2 are determined from a measurement of the scattered electron in the backward drift chamber (BDC) and the lead-scintillating fibre calorimeter (SPACAL). Jets are reconstructed using the information provided by the central tracking chambers and the liquid argon calorimeter (LAr).

Electrons are identified through their energy deposits in the SPACAL electromagnetic calorimeter and related hits in the BDC. The scattering angle of the electron can be determined from the reconstructed primary vertex and the measured impact position in the BDC. The BDC covers the angular range $153^o < \theta < 177^o$ and gives an accuracy of $\Delta\theta < 0.5$ mrad.

The SPACAL electromagnetic calorimeter is a lead/scintillating-fibre detector with a depth of 28 radiation lengths. The energy resolution is $\sigma/E = 7\%/\sqrt{E} \oplus 1\%$, with E in GeV.

The central tracking system has been designed to reconstruct jets with high particle densities and to measure the momentum and direction of isolated charged particles to a precision of

$\sigma_p/p^2 \approx 3 \cdot 10^{-3}$ GeV^{-1} and $\sigma_\theta \approx 1$ mrad. The track reconstruction is done in two concentric jet chambers (CJC1 and CJC2) with wires oriented parallel to the beam axis. Two thin drift chambers, one inside CJC1 and one between the CJC1 and the CJC2, have their wires perpendicular to the beam direction and provide the z-coordinates of the tracks. Two proportional chambers next to the thin drift chambers provide a fast trigger signal for central tracks.

The main calorimeter is a sandwich type calorimeter with liquid argon as the active material. It covers a range in polar angle of $4^o < \theta < 153^o$. The electromagnetic energy resolution varies between $\sigma/E = 10\%/\sqrt{E}$ and $13\%/\sqrt{E}$ (E in GeV) with a constant term below 1%, whereas the hadronic energy resolution is $\sigma/E = 50\%/\sqrt{E}$ (E in GeV) with an energy independent term of less than 2%.

The luminosity is determined from the measured rate of elastic Bremsstrahlung scattering, $e + p \rightarrow e + \gamma + p$ (Bethe-Heitler events), with a luminosity monitor consisting of two arms. The electron tagger is placed next to the beam pipe at a distance of 33 m from the nominal interaction point, whereas the photon detector is situated at 103 m distance in the direction of the incoming electron beam.

In this analysis a combination of two triggers is used. Both are based on energy deposition in the SPACAL detector. The combination of triggers results in a trigger efficiency of $\sim$100%.

5 Event Selection

The ep scattering data studied here were collected in 1997 at $\sqrt{s} \sim 300$ GeV with the H1 detector and comprise an integrated luminosity of $13.7\ \mathrm{pb}^{-1}$.

DIS events are selected by requiring a scattered electron in the backward SPACAL calorimeter with an energy $E'_e > 10$ GeV in the angular range of $156^\circ < \theta_e < 175^\circ$. The cuts, which are applied in the laboratory frame, are summarized below:

$$
\begin{gathered}
E_{e'} > 10 \text{ GeV} \\
156^\circ < \theta_e < 175^\circ \\
0.1 < y < 0.7 \\
0.0001 < x_{Bj} < 0.004 \\
5 \text{ GeV}^2 < Q^2 < 85 \text{ GeV}^2 \, .
\end{gathered}
$$

Here E'_e and θ_e are the energy and the scattering angle of the scattered electron, respectively. These variables are determined from the scattered electron.

The forward jets are defined using the k_t-jet algorithm [12] in its inclusive mode (applied in the Breit-frame) and by requiring (in the laboratory frame):

$$
\begin{gathered}
p_{t,jet} > 3.5 \text{ GeV} \\
7.0^o < \theta_{jet} < 20.0^o \\
x_{jet} > 0.035 \, .
\end{gathered}
$$

6 Monte Carlo Programs

The H1 data have been compared to the predictions of several Monte Carlo programs. The RAPGAP [13] Monte Carlo model (labeled RG) uses LO matrix elements supplemented with initial and final state DGLAP parton showers for the description of typical DIS-processes (DGLAP direct). It is interfaced to HERACLES [15] in order to simulate QED-radiative effects. RAPGAP also offers the possibility to include contributions from resolved virtual photon processes (DGLAP resolved). In the analysis we have used the DJANGO [14] program, which provides an interface to HERACLES, with the colour dipole model (CDM) as implemented in ARIADNE [16]. The CASCADE Monte Carlo program [17] is based on the CCFM formalism. Two different versions of the unintegrated gluon density were used, J2003-set-1 and set-2. The difference between these two sets is that in set-1 only singular terms were included in the splitting function, whereas set 2 also takes the non-singular terms into account. The unintegrated gluon densities have been determined from fits to the $F_2(x, Q^2)$ data obtained by H1 and ZEUS in 1994 and 1996/97 [18]. Simulated events from the RG-DIR and DJANGO Monte Carlo programs have been processed through the detailed H1 detector simulation in order to test the understanding of the detector and make acceptance corrections.

A comparison is also made to NLO calculations as obtained by using the DISENT program. These calculations are corrected for hadronization effects, which are estimated by using CASCADE together with the KMR parton density function. The KMR parton density function takes only the hard scattering vertex and one additional emission into account and should therefore be suitable for correcting the NLO calculations.

7 Control Plots and Correction Factors

The extent to which the selection of DIS events and the forward jet sample could be reproduced by the Monte Carlo programs was investigated through a comparison of data with predictions from the DGLAP-direct model and the CDM model. The quality of the DIS selection and the absolute normalization was checked by comparing the distributions of DIS events for data and the models as a function of the kinematic variables x_{Bj}, y, Q^2 and the energy and polar angle of the scattered electron (E'_e and θ_e). Excellent agreement was observed for both models in all distributions. In Fig. 3 the distributions of x_{Bj}, E'_e and θ_e are shown.

For the forward jet selection the distributions of the jet azimuthal angle (ϕ_{jet}), the jet rapidity (η_{jet}), the jet transverse momentum ($p_{t,jet}$), the ratio $p^2_{t,jet}/Q^2$ and the fractional jet energy $x_{jet} = E_{jet}/E_p$ were examined. The distributions of the DIS kinematic variables for the forward jet sample are reproduced better by the CDM model than by DGLAP-direct, whereas for the forward jet variables the DGLAP-direct model gives a somewhat better agreement with data than the CDM model, as shown in Fig. 4

The hadron level cross sections were extracted by applying correction factors to the data which take detector effects into account. The correction factors were calculated as the ratio of the Monte Carlo prediction at the hadron- and detector levels, in a bin-by-bin procedure. RAPGAP and CDM gave very similar values over the full kinematic range covered in this

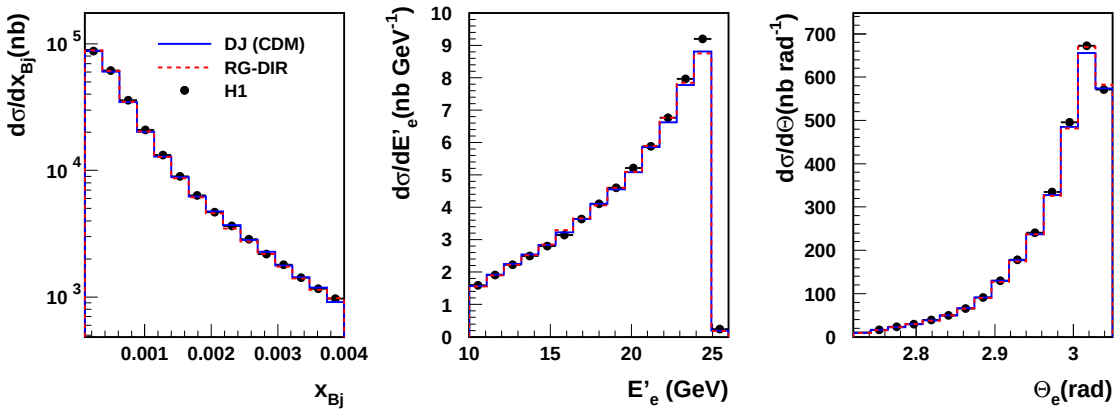

Figure 3: *Control plots for the DIS selection. The distributions are normalized according to the luminosity.*

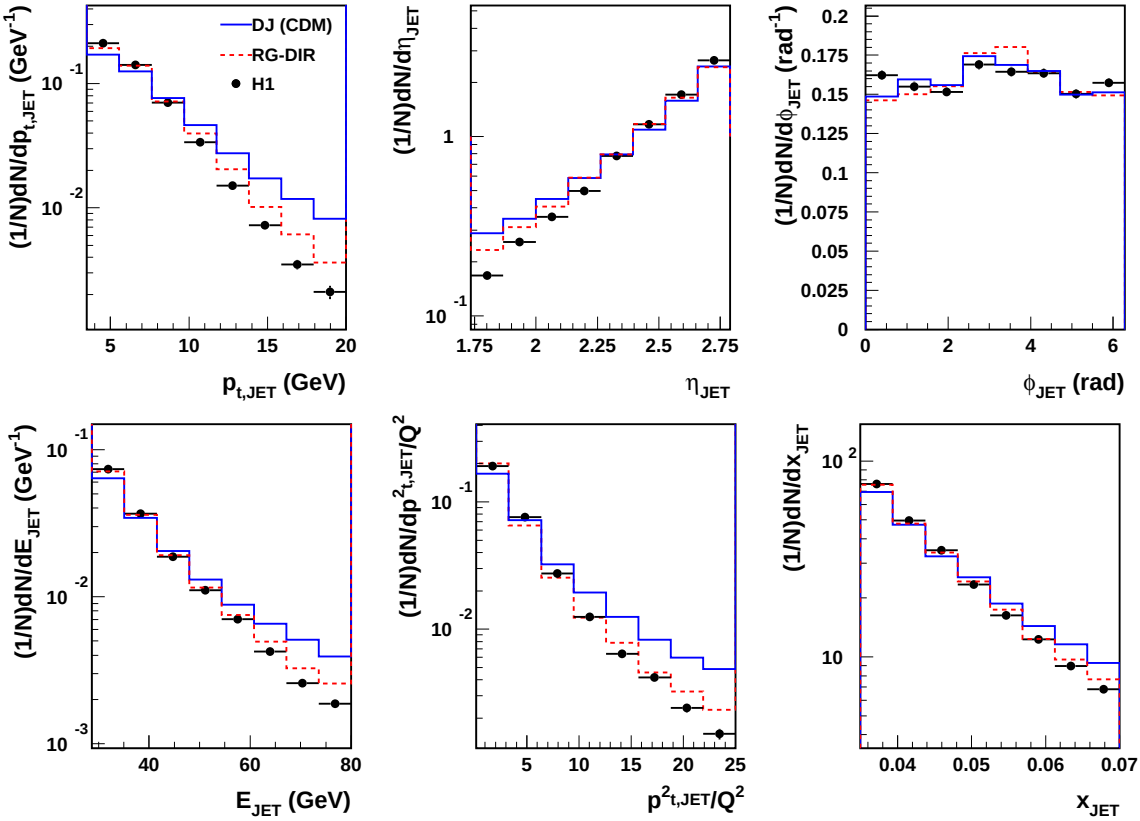

Figure 4: *Control plots for the forward jet variables, when no $p^2_{t,jet}/Q^2$-cut is applied. The distributions are normalized to unity. All variables are measured in the laboratory frame.*

investigation. The CDM model was finally used to correct data from the detector level to the hadron level. The correction factors vary between 0.7 and 1.2 but in a few cases reach 0.5 or 1.4. The variations in the corrections factors from the two Monte Carlo models are included in

the systematic error. The purity and acceptance[1] were found to be larger than 30% in all bins. For the 2+forward jet analysis they are larger than 40% in all bins.

7.1 Systematic Uncertainties

The systematic errors have been estimated for each data point separately. In the figures the quadratic sum of the errors is shown. The total systematic errors are 10%, 12% and 14% for the inclusive, triple and the 2+forward jet cross section, respectively. The following systematic errors are considered:

- The energy calibration of the hadronic calorimeter has been performed to a precision of $\pm 4\%$. In order to estimate the dependence of the measured forward jet cross section on this uncertainty, the energy scale was changed within these limits and the influence on the forward jet cross section was calculated using the DJANGO generator. The average systematic error is typically 8% for the inclusive forward jet cross section and the triple differential forward jet cross section.
- For the SPACAL electromagnetic calorimeter the energy scale is known to an accuracy of $\pm 1\%$. Changing the scale by this amount in the forward jet cross section calculations results in an average systematic error of typically 3%.
- The uncertainty on the measured scattering angle of the electron has been estimated to be ± 1 mrad. The systematic error which we get by implementing this measurement uncertainty in the DJANGO forward jet cross section calculation is typically 1%.
- The error from the model dependence has been taken as the difference between the correction factors calculated from the DJANGO and the RG-DIR Monte Carlo programs. Taking this variation into account yields a systematic error of around 5% in the inclusive case and 8% for the triple differential forward jet cross section.
- The PHOJET [19] Monte Carlo generator was used in order to estimate the extent to which DIS forward jet events could be faked by photoproduction background. The contribution to the forward jet cross section was calculated to be ~ 1%.
- The normalization uncertainty of the luminosity measurement has been estimated to be 1.5%.

8 Results

8.1 Inclusive Forward Jet Production

The first measurement concerns the inclusive production of forward jets in deep inelastic scattering. The events were selected by implementing the requirements described in section 5.

[1]The purity (acceptance) is obtained from the same Monte Carlo simulations as for the correction factors and is defined as the fraction of events reconstructed (generated) in a bin that were also generated (reconstructed) in that bin.

Following the discussion in section 3 on how to suppress the phase space for DGLAP evolution the requirements $0.5 < p^2_{t,jet}/Q^2 < 5$ and $x_{jet} > 0.035$ GeV were applied. Lowering the upper $p^2_{t,jet}/Q^2$ cut leads to poor purities. This is caused by the limitations of the detector resolution in the $p_{t,jet}$ measurement.

In Fig. 5a the inclusive forward jet cross section is shown as a function of x_{Bj} and compared to the prediction of NLO calculations from DISENT. In Fig. 5b data are compared to the various QCD models.

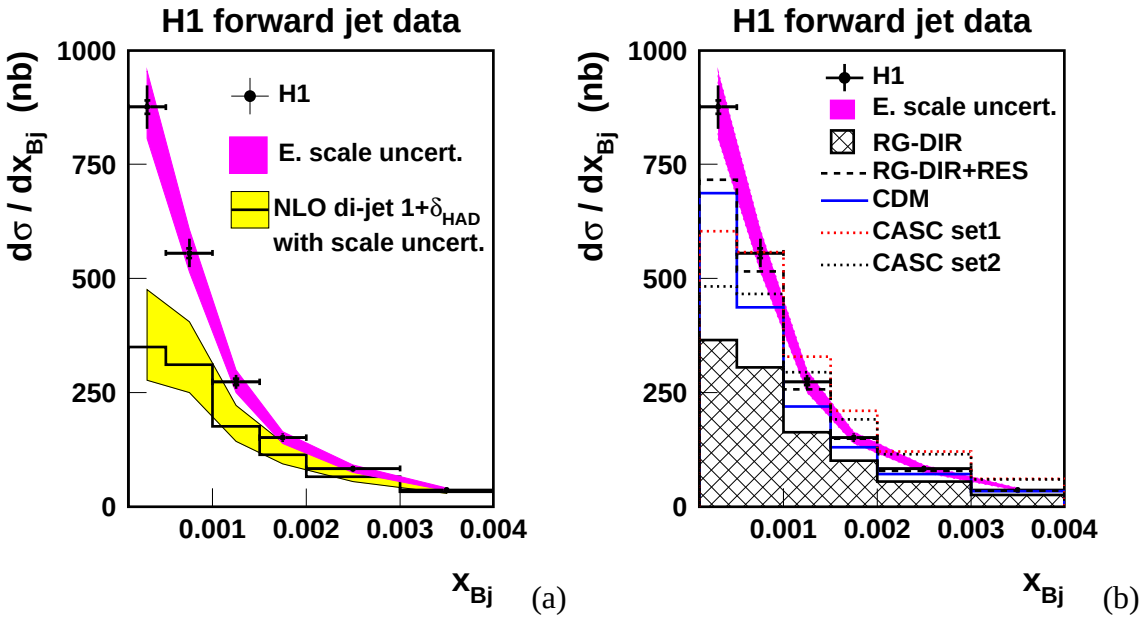

Figure 5: *The hadron level cross section for inclusive forward jet production as a function of x_{Bj} compared to the prediction of (a) NLO calculations and (b) QCD Monte Carlo models. The band following the data points shows the uncertainty from variation of the energy scales of the liquid argon calorimeter, the SPACAL electromagnetic calorimeter and the luminosity monitor. The band following the NLO calculations illustrates the scale uncertainty in the calculations, estimated as described in the text.*

The NLO calculations were performed using the CTEQ6M parametrization of the proton parton densities with the renormalization scale given by the E^2_T of the jet. The average E^2_T of the jets (45 and 67 GeV^2 for the inclusive and the triple differential cross sections, respectively) was used as the factorization scale. The scale uncertainty was estimated by changing the scale by a factor of four, $E^2_T/4 < \mu^2_r < 4E^2_T$, and is indicated as a band in the plot. The parametrization of the parton densities and the scale used in the QCD models are given in table 1.

From the figures it is obvious that the DGLAP model with direct photon interactions alone (RG-DIR) and the NLO calculation both fall below the data: This is especially pronounced at low x_{Bj}. The somewhat improved agreement at higher x_{Bj} can be understood from the fact that the range in the longitudinal momentum fraction which is available for higher order emissions is decreased due to the x_{jet} cut. The description of the data by the DGLAP-model is

significantly improved if contributions from resolved virtual photon interactions are included (RG-DIR+RES). However, there is still a discrepancy in the lowest x_{Bj}-bin, where a possible BFKL signal would be expected to show up most prominently. The CDM model, which gives emissions that are non-ordered in transverse momentum, shows a similar behaviour to the RG DIR+RES model. In addition the CCFM-model (with both set-1 and set-2 partons) predicts a somewhat different shape for the x_{Bj} distribution, which results in a comparatively poor description of the data.

	CASCADE	RG-DIR	RG-RES	DISENT
μ_r^2	$m^2 + p_{t,jet}^2$	$Q^2 + p_{t,jet}^2$	$Q^2 + p_{t,jet}^2$	$\frac{1}{4}p_{t,jet}^2 < p_{t,jet}^2 < 4p_{t,jet}^2$
μ_f^2	Determined by Ξ	$Q^2 + p_{t,jet}^2$	$Q^2 + p_{t,jet}^2$	$< p_{t,jet}^2 > (= 45$ resp. 67 GeV$^2)$
proton pdf	J2003 set 1 & 2	CTEQ6L	CTEQ6L	CTEQ6M
photon pdf	-	-	SaS1D	-

Table 1: *Scales and parton density functions used in the different generators. Ξ denotes the maximum emission angle given by the quark box determining the factorization scale.*

8.2 Triple Differential Cross Sections

In order to get a more complete picture of forward jet production the data are also presented as triple differential cross sections. The total forward jet event sample was subdivided into bins of Q^2 and $p_{t,jet}^2$. The triple differential cross section $\frac{d\sigma}{dx_{Bj}dQ^2dp_{t,jet}^2}$ versus x_{Bj} is shown in Figs. 6 and 7 for three regions in Q^2 and $p_{t,jet}^2$. In Fig. 6 the data are compared to the DISENT NLO calculations, whereas in Fig. 7 comparisons to the Monte Carlo models are shown. The same parton density functions and scales have been used as in the inclusive case. Again the scale uncertainty is represented by a band in Fig. 6.

From Fig. 6 it can be observed that the NLO calculations, within the fairly large scale uncertainty, agree with the data in the regions of high Q^2 and/or high $p_{t,jet}^2$. For lower values of these parameters the NLO calculations fall below the data. This is consistent with the results from a previous measurement on inclusive jet production [20].

The kinematic region covered in Figs. 6c and 7c includes the case where Q^2 is larger than $p_{t,jet}^2$, which is typical for direct photon interactions, but it extends into the region where Q^2 is approximately equal to or even smaller than $p_{t,jet}^2$, and where emissions non-ordered in virtuality are expected. This could explain why the DGLAP direct model (RG-DIR) does not give a good description of the data except for the highest x_{Bj}-bin. The CDM model reproduces the data very well and the DGLAP resolved model (RG-DIR+RES) is also in reasonable agreement. The CCFM model (CAS1 and CAS2) overshoots the data over the full x_{Bj}-region.

Figs. 6d, e, g, h and i, and 7d, e, g, h and i cover a kinematic region where $p_{t,jet}^2$ is larger than Q^2, which is typical for processes where the virtual photon is resolved. As expected the DGLAP resolved model (RG-DIR-RES) a good overall good description of the data, whereas

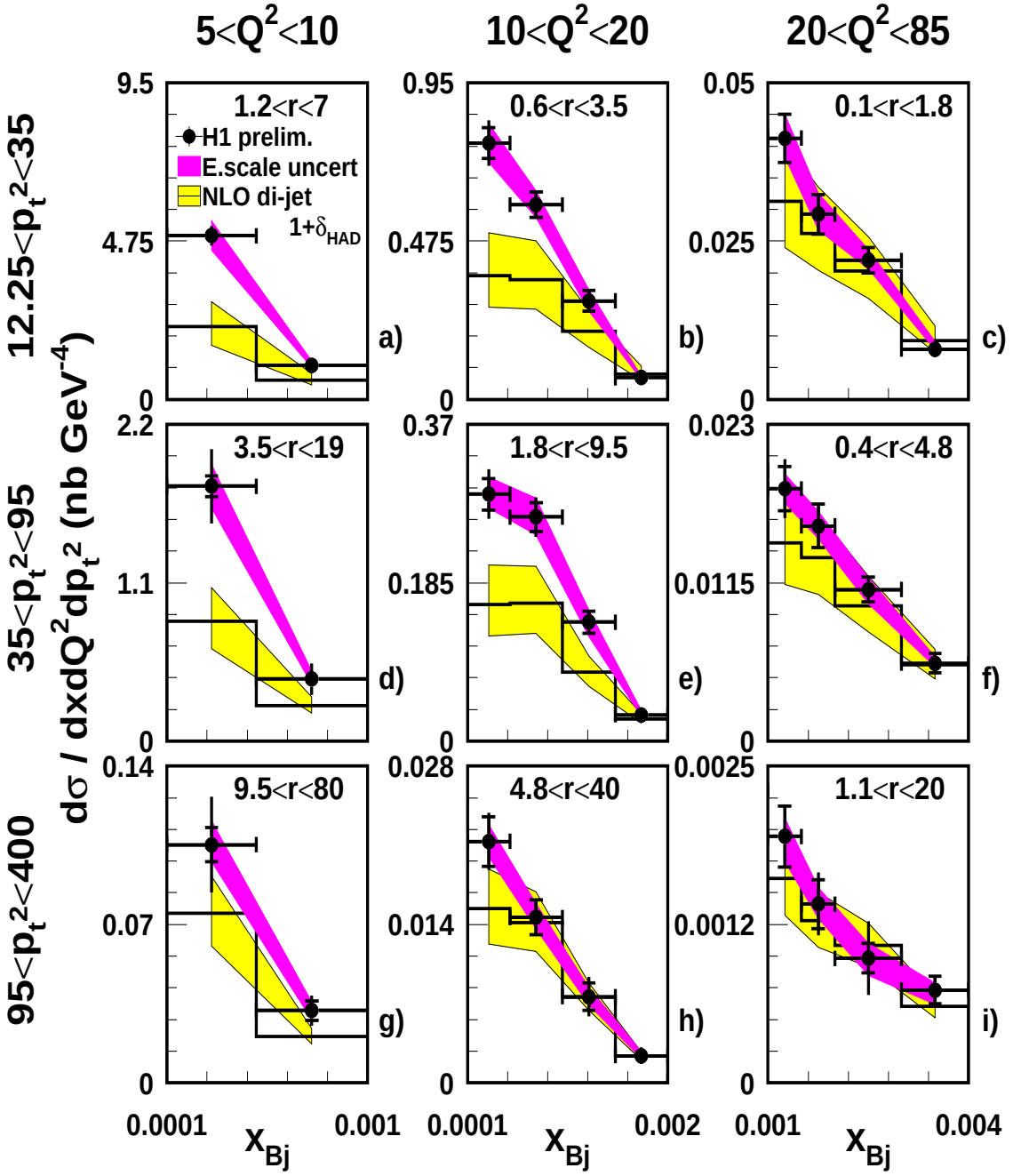

Figure 6: *The hadron level triple differential cross section for forward jet production as a function of x_{Bj}, in bins of Q^2 and $p^2_{t,jet}$. The data are compared to the prediction of NLO calculations. The band following the data points illustrates the uncertainty due to variation in the energy scales of the liquid argon calorimeter, the SPACAL electromagnetic calorimeter and the luminosity monitor. The band following the NLO calculations illustrates the scale uncertainty in the calculations. In every bin the coverage in $r = p^2_{t,jet}/Q^2$ is shown.*

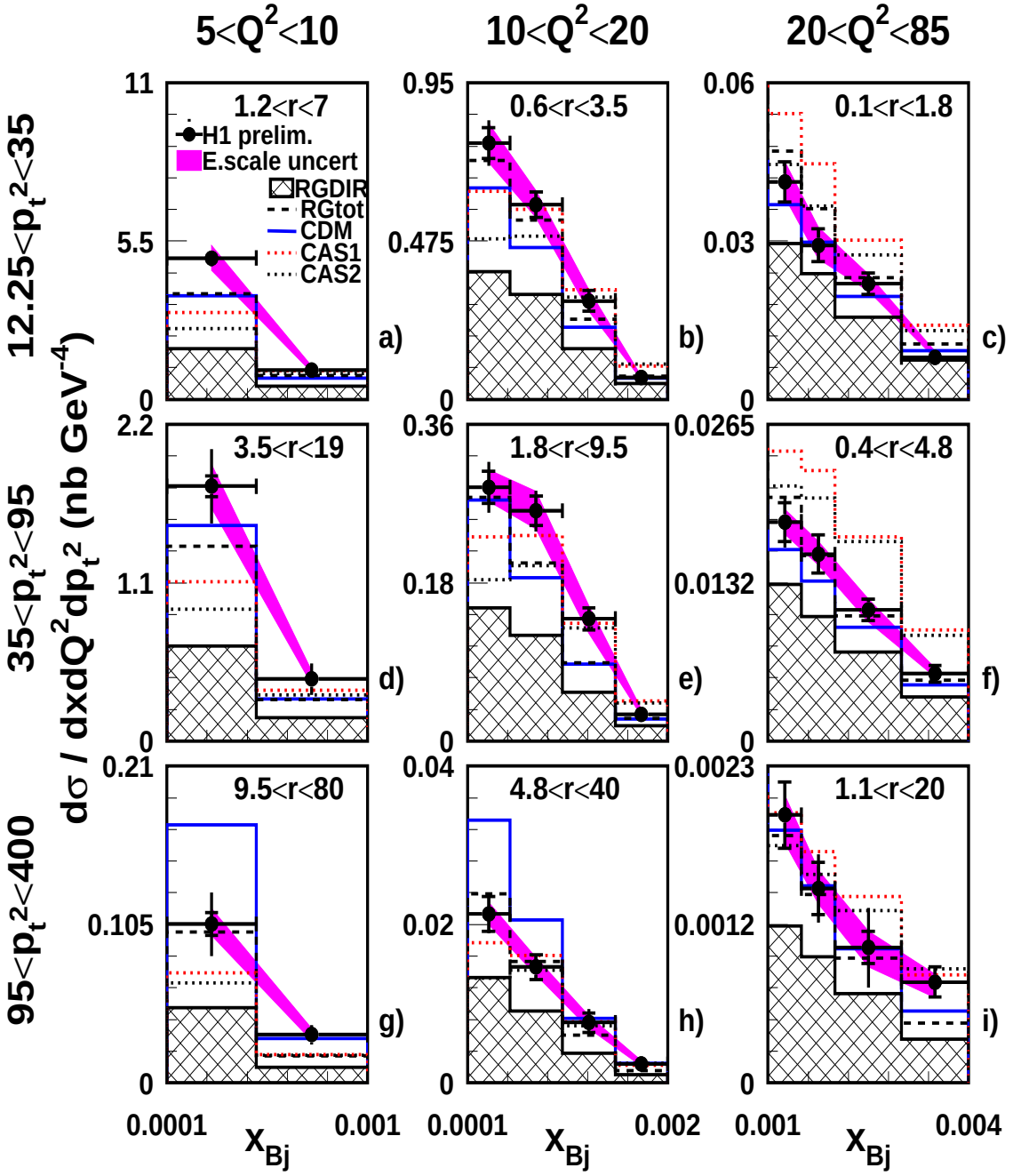

Figure 7: *The hadron level triple differential cross section for forward jet production as a function of x_{Bj}, in bins of Q^2 and $p^2_{t,jet}$. The data are compared to the prediction of QCD Monte Carlo models. The band following the data points illustrates the uncertainty in the energy scales of the liquid argon calorimeter, the SPACAL electromagnetic calorimeter and the luminosity monitor. In every bin the coverage in $r = p^2_{t,jet}/Q^2$ is shown. RG-DIR+RES is here denoted by RGtot.*

DGLAP direct (RG-DIR) and NLO calculations give cross sections which are generally too low. The CDM-model overshoots the data significantly at high values of $r = \frac{p^2_{t,jet}}{Q^2}$ and small values of x_{Bj}.

The "BFKL region", with $p^2_{t,jet}$ of the same order as Q^2, is represented by Figs. 6b and f, and 7b and f, where Figs. 6b and 7b cover the lower range in $p^2_{t,jet}$ and Q^2 and Figs. 6f and 7f the higher range. In this kinematic region the data are best described by the DGLAP resolved (RG-DIR+RES) model, whereas the CDM model gives somewhat too low cross-sections. In the bin of low $p^2_{t,jet}$ and Q^2 (Fig. 7b) there is a tendency for CCFM (CAS1 and CAS2) to underestimate the production cross section at low values of x_{Bj} and overestimate it at higher values, as was already observed in the inclusive distribution. For low values of $p^2_{t,jet}$ and high Q^2 (Fig. 7c, f) the CCFM predictions are significantly too high over the full x_{Bj}-range.

8.3 Events with Reconstructed Di-jets in Addition to the Forward Jet

Complementary to the analysis reported in section 8.1 and 8.2, where the $p^2_{t,jet}/Q^2$ cut was used to enhance a possible BFKL signal, we also used another method to control the evolution kinematics. By requiring the reconstruction of two jets in the central region of the detector, we can investigate different kinematic regions by applying cuts on the jet momenta and their rapidity separation as described in more detail in section 3.

Di-jets from the central region were found by applying the inclusive k_t-jet algorithm in the Breit frame and demanding that jets have transverse momenta larger than 6 GeV. The jets are ordered in rapidity according to $\eta_{fwd-jet} > \eta_{jet_2} > \eta_{jet_1} > \eta_e$ with η_e being the rapidity of the scattered electron, see Fig. 2. The cross section is measured in two intervals of $\Delta\eta_1 = \eta_{jet_2} - \eta_{jet_1}$. By applying the same $p_{t,jet}$ cut for all three jets, evolution with strong k_t-ordering is suppressed. In order to maximize the phase space available for BFKL evolution $\Delta\eta_1 < 1$ was required. This means that the invariant mass of the di-jet system and x_g are small (see Fig. 2). A consequence of this is that the rapidity difference of the di-jet system to the forward jet is maximized. On the other hand, by demanding $\Delta\eta_1 > 1$ we select di-jet systems with higher invariant masses and larger x_g; the separation of the di-jet system and the forward jet becomes smaller and a description corresponding to the resolved photon picture should become adequate. In this investigation no comparison with NLO(α_s^2)-calculations is made since these by construction are limited to the production of three jets. The same versions of the QCD models were used as in the previous studies.

The cross section for events containing a di-jet system in addition to the forward jet is shown in Fig. 8, as a function of $\Delta\eta_2 = \eta_{fwd-jet} - \eta_{jet_2}$ for all jets, and for the requirements $\Delta\eta_1 < 1$ and > 1. The cross section $d\sigma/d\Delta\eta_2$ for $\Delta\eta_1 < 1$ is found to be fairly well described by the CASCADE MC with set-2 parton densities except in the lowest bin where all models fail. This is the bin where the rapidity range for additional radiation is the smallest. CASCADE with set-1 partons, however, gives too high cross section values in the two highest $\Delta\eta_2$ bins. The DGLAP direct and resolved models are both significantly below the data in the whole range. In the sample where $\Delta\eta_1 > 1$, the data are not described by any model in the lowest $\Delta\eta_2$-bin, while for the two other bins both CASCADE set-1 and set-2 give cross sections that are too large. The DGLAP models give good agreement in the highest $\Delta\eta_2$-bin. The observed behaviour is

consistent with that expected from the discussion above. Within the uncertainty in the energy scale, the CDM model gives somewhat better agreement with data for $\Delta\eta_1 < 1$ (the BFKL region) than for $\Delta\eta_1 > 1$ (the resolved region), where it fails to reproduce the lowest $\Delta\eta_2$ bin.

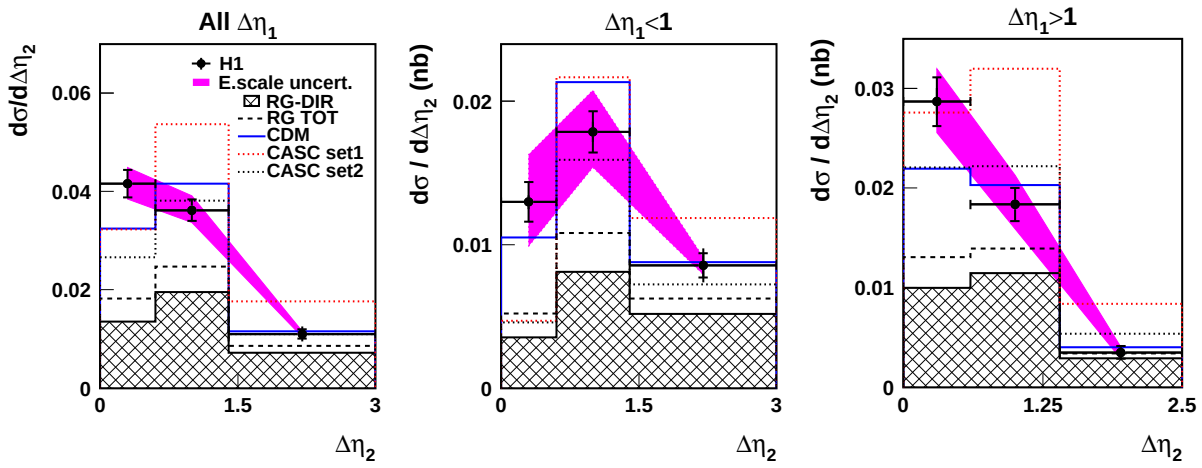

Figure 8: *The cross section for events with a reconstructed high transverse momentum central di-jet system and a forward jet as a function of the rapidity gap between the forward jet and the most forward-going central jet, $\Delta\eta_2$. Results are shown for the full sample and for two ranges of the separation between the two central jets, $\Delta\eta_1 < 1$ and $\Delta\eta_1 > 1$. The data are compared to the predictions of QCD Monte Carlo models.*

9 Conclusion

An investigation of DIS events containing a jet in the forward direction has been performed using data collected in 1997, comprising an integrated luminosity of 13.72 pb^{-1}. Various constraints have been applied which suppress contributions to the parton evolution described by the DGLAP equations and thus enhance the sensitivity to new parton dynamics. Several observables involving forward jet events have been studied and compared to the predictions of NLO calculations and QCD models.

The results on inclusive forward jet production show that NLO calculations and the DGLAP direct model give cross sections which are consistently below the data at small values of x_{Bj}. The DGLAP resolved photon model and colour dipole model give the best description of the data, whereas the CCFM model, studied with two different parametrizations of the unintegrated gluon density, does not reproduce the shape of the distribution. This shows that the forward jet cross section is sensitive to the details of the unintegrated gluon density and can be used to further constrain this density.

The total forward jet sample was subdivided into bins of Q^2 and $p^2_{t,jet}$ such that kinematic regions were defined in which different evolution dynamics were expected to dominate. At high

Q^2, ($Q^2 \gg p_{t,jet}^2$) the most DGLAP like region, the data are described by NLO calculations within the scale uncertainty. In the region where contributions from resolved processes are expected to become important ($p_{t,jet}^2 \gg Q^2$) we find good agreement with the DGLAP resolved model but the cross sections predicted by the NLO calculations and DGLAP direct model are too low. In this region the CDM tends to overshoot the data. In the BFKL region ($Q^2 \sim p_{t,jet}^2$) the CCFM model does not manage to describe the shape of the distributions and CDM and DGLAP resolved reproduce the data best.

The study of events with a reconstructed central di-jet system in addition to the forward jet reveals reasonably good agreement with CASCADE in the region where BFKL evolution is expected to dominate. In the region where we expect resolved photon processes to become important the DGLAP resolved model is closer to the data

The observations made here demonstrate that an accurate description of the radiation pattern at small x_{Bj} requires the introduction of terms beyond those present in the collinear DGLAP approximation. Higher order parton emissions with significant transverse momentum contribute noticeably to the cross section. Calculations which include these processes, such as CCFM, CDM and the resolved photon model, provide a better description of the data.

References

[1] V. Gribov and L. Lipatov, *Sov. J. Nucl. Phys.* **15**, 438 and 675 (1972)
L. Lipatov, *Sov. J. Nucl. Phys.* **20**, 94 (1975)
G. Altarelli and G. Parisi, *Nucl. Phys.* **B 126**, 298 (1977)
Y. Dokshitzer, *Sov. Phys. JETP* **46** 641 (1977)

[2] G. Gustafson, *Phys. Lett.* **B 175**, 453 (1986)
G. Gustafson, U. Pettersson *Nucl. Phys.* **C 306**, 746 (1988)

[3] H1 Collab., A. Aktas et al. DESY-03-206 (Jan 2004) 32p. [HEP-EX 0401010]

[4] S. Catani, M.H. Seymour, *Phys. Lett.* **B 378**, 287 (1996), *Nucl. Phys.* **B 485**, 291 (1997)

[5] H. Jung, L. Jönsson, H. Küster, *Eur. Phys. J.* **C 9**, 383 (1999)

[6] E. Kuraev, L. Lipatov and V. Fadin, *Sov. Phys. JETP* **44**, 443 (1976)
E. Kuraev, L. Lipatov and V. Fadin, *Sov. Phys. JETP* **45**, 199 (1977)
Y. Balinsky and L. Lipatov, *Sov. J. Nucl. Phys.* **28**, 822 (1978)

[7] M. Ciafaloni, *Nucl. Phys.* **B 296**, 49 (1988)
S. Catani, F. Fiorani and G. Marchesini, *Phys. Lett.* **B 234**, 339 (1990)
S. Catani, F. Fiorani and G. Marchesini, *Nucl. Phys.* **B 336**, 18 (1990)
G. Marchesini, *Nucl. Phys.* **B 445**, 49 (1995)

[8] A. Mueller, *Nucl. Phys.* **B** (*Proc. Suppl*) **18C** 125 (1990)
A. Mueller, *J. Phys.* **G 17**, 1443 (1991),

[9] H1 collaboration, C. Adloff et al., *Nucl. Phys.* **B 538**, 3 (1999)

[10] H1 collaboration, Forward π^o Production in DIS at HERA, Contributed paper to the International Europhysics Conference on High Energy Physics, EPS03, July 17-23, Aachen, Germany and XXi International Symposium on Lepton and Photon Interactions, LP03, August 11-16, 2003, Fermilab, USA.

[11] H1 collaboration, I. Abt et al., *Nucl. Instrum. Methods* **A 386**, 310 and 348 (1997)

[12] S. Catani, Y. Dokshitzer, M. Seymour, B. Webber, *Nucl. Phys.* **B 406**, 187 (1993)
S. Catani, Y. Dokshitzer, B. Webber, *Phys. Lett.* **B 285**, 291 (1992)

[13] H. Jung, *Comp. Phys. Comm.* **143**, 100 (2002)

[14] K. Charchula, G.A. Schuler, H. Spiesberger, *Comp. Phys. Comm.* **81**, 381 (1994)

[15] A. Kwiatkowski, H. Spiesberger, H.-J. Möhring *Comp. Phys. Comm.* **69**, 155 (1992)

[16] L. Lönnblad, *Comp. Phys. Comm.* **71**, 15 (1992)
L. Lönnblad, *Z. Pys.* **C 65**, 285 (1995)

[17] H. Jung, G. Salam *Eur. Phys. J.* **C 19**, 351 (2001)
H. Jung, *Comp. Phys. Comm.* **143**, 100 (2002)

[18] M. Hansson, H. Jung, hep-ph/0309009

[19] R. Engel, *Z. Phys.* **C 66**, 203 (1995)
R. Engel, J. Ranft, *Phys. Rev.* **D 54**, 4244 (1996)

[20] H1 Collab., C. Adloff et al., Phys. Lett. **B 542** 193 (2002)